

DIONYSOS: A diagnostic tool for numerically-simulated
weather systems

by

Jean-François Caron,
Peter Zwack
and Christian Pagé

Department of Earth and Atmospheric Sciences
Université du Québec à Montréal
Montréal, Québec
Canada

November 2006

Corresponding author address:

Jean-François Caron
Atmospheric Science and Technology Directorate
Environment Canada
2121 route Transcanadienne, Dorval, Québec
Canada, H9P 1J3

E-mail: jean-francois.caron@ec.gc.ca

Abstract

DIONYSOS is a diagnostic package specifically adapted to standard output from numerical weather prediction models that runs daily at the Canadian Meteorological Centre (CMC). It allows for the interpretation of significant parameters related to weather systems such as development (vorticity, geostrophic vorticity and height tendencies), vertical motion, divergence and temperature tendencies. It is based on primitive omega, vorticity, and thermodynamic equations as well as the nonlinear balance equation. The current version of DIONYSOS computes the contributions of individual dynamical and thermodynamical forcings to the parameters mentioned above. These forcings include vorticity and temperature advections, latent and sensible heating, friction and orography. In addition, contributions from specific regions of the atmosphere can be computed separately. Because some of the forcings are not available from standard model output, they are parameterized using available fields. A complete description of the diagnostic equations, parameterizations and computational techniques is presented. To evaluate the diagnostic performance, statistical quantities are calculated for a pair of nine synoptic times from two 24-hour simulations: a winter case and a summer case. Results show that DIONYSOS total diagnostic fields (i.e. the sum of contributions from each forcing) of the tendencies of vorticity, geostrophic vorticity, temperature and height, as well as the vertical motion, show good agreement with the original model fields.

1. Introduction

Ever since the development of extended surface and upper-air observations networks and the era of numerical weather simulations, diagnostic equations have been developed in order to better understand the structure and evolution of weather systems. Over time, less restrictive approximations have been used which enables a better identification of the key features in an extremely complex atmosphere. This has led to an increase in our knowledge of weather systems.

In the middle of the twentieth century, the Sutcliffe development equation (Petterssen 1956, p.324) was derived for diagnosing surface geostrophic vorticity tendency. It required the use of a level of non-divergence as well as the quasi-geostrophic (QG) framework, which limited its usefulness to be of a qualitative nature. Holton (1992, p.159) presented a QG height tendency equation that, again, was useful only qualitatively because of the need of upper and lower boundary conditions. Following Zwack and Okossi's (1986) QG development equation (Z-O equation) where diabatic effects were included, Lupo *et al.* (1992) developed an extended version of the Z-O equation which made use of the total wind and total vorticity and included frictional effects. However, the ageostrophic vorticity tendency was neglected and the vertical motion was considered an independent forcing mechanism.

To avoid using the QG approximation, Räisänen (1997, hereafter R97) developed a diagnostic method, similar to Krishnamurti (1968), based on the primitive equations. Using a generalized omega equation (Räisänen 1995, hereafter R95) and the full vorticity equation, this approach allows for the partitioning of vertical motion, vorticity tendency

and height tendency into contributions from various forcings including diabatic heating and friction, and where vertical motion is formally eliminated as an independent forcing. However, R97 considered the ageostrophic vorticity tendency as an independent dynamical process.

The approach presented here adopts R97's diagnostic approach except that ageostrophic vorticity tendencies are eliminated as an independent forcing by using the nonlinear balance approximation (Charney 1955). Using this framework can potentially help to reduce possible ambiguities in the interpretation of the physical processes involved, because these diagnostic equations are using only nonlinear balance and hydrostatic approximations. This is an improvement over the QG approximation.

Complementary equations to R97 diagnostics were also added to compute individual forcings contributions to temperature and geostrophic vorticity tendencies, and to divergence. These equations are all included in DIONYSOS diagnostic software that was specifically developed to be applicable to standard output of numerical weather prediction (NWP) models. This diagnostic package, run twice daily at the Canadian Meteorological Centre, allows for the synoptic and dynamic interpretation, inter-comparison and verification of model forecasts on a real-time and retrospective basis. DIONYSOS is unique in that it can be run using only standard output from most of NWP models, ensuring its applicability to a variety of modeling systems. For example, DIONYSOS diagnostics are run daily at the Université du Québec à Montréal on output from the Canadian (GEM) and American (GFS) Global models over North America, Europe, and New Zealand as well as the NAM over North America. This was made

possible by developing parameterizations of the forcings that would have required special model output.

The present paper describes this diagnostic package. The DIONYSOS diagnostic equation set is presented in section 2. The new treatment of the ageostrophic vorticity tendency term in the omega equation is presented in section 3. Section 4 describes the parameterization of the forcings. Quantitative comparisons between diagnostic fields and model data for two different cases are presented in section 5, while section 6 provides a summary and discussions of future plans. Finally, a description of the data processing as well as a list of the data required for the diagnostics can be found in appendix A

2. Diagnostic equations

DIONYSOS is based on a complete ensemble of hydrostatic primitive diagnostic equations that are solved using the nonlinear balance approximation. The basic equation set is composed of the omega, vorticity, thermodynamic and nonlinear balance equations.

a. Omega equation – Vertical motion

Equation 1 is the complete hydrostatic omega equation in pressure coordinates from R95, where the symbols have their usual meteorological meaning (e.g., Holton 1992, p.476-479) except for \mathbf{F} which represents frictional forcing and the subscript AG that refers to ageostrophic terms:

$$\begin{aligned}
& \frac{R}{p} \nabla^2 S \omega + f(f + \zeta) \frac{\partial^2 \omega}{\partial p^2} - f \omega \frac{\partial^2 \zeta}{\partial p^2} - f \frac{\partial}{\partial p} \left(\frac{\partial \omega}{\partial x} \frac{\partial v}{\partial p} - \frac{\partial \omega}{\partial y} \frac{\partial u}{\partial p} \right) \\
& = -\frac{R}{p} \nabla^2 (-\mathbf{V} \cdot \nabla T) - \frac{R}{p} \nabla^2 \frac{\dot{q}}{c_p} - f \frac{\partial}{\partial p} [-\mathbf{V} \cdot \nabla (f + \zeta)] \\
& - f \frac{\partial}{\partial p} (\mathbf{k} \cdot \nabla \times \mathbf{F}) + f \frac{\partial}{\partial p} \left(\frac{\partial \zeta_{AG}}{\partial t} \right)
\end{aligned} \tag{1}$$

This equation can be derived from the primitive equations (motion, energy, ideal gas and continuity) with only the hydrostatic approximation (see Pagé *et al.* (2007) for a complete derivation of this equation). On the right-hand side, the five forcing terms represent the Laplacian of temperature advection (*LTA*), Laplacian of diabatic heating (which is, in DIONYSOS, divided only into a Laplacian of sensible heating (*LSH*) and a Laplacian of latent heat release (*LLH*)), vorticity advection (*VA*), friction (*FR*) and an ageostrophic vorticity tendency (*AG*) term. In section 3, the method for partitioning the *AG* term among the other forcing contributions is explained. Given that the left-hand side of (1) is linear with respect to ω , the contributions to vertical motion of the independent forcings can be calculated separately by imposing homogenous conditions ($\omega=0$) on all (lateral, upper and lower) boundaries. Orographical effects (*OR*) on vertical motion are also computed in DIONYSOS by imposing a diagnosed surface orographic vertical motion (obtained from horizontal winds and topography) as the lower boundary condition in (1) and then solving the equation with all forcing terms and the vertical motion on the upper and lateral boundaries set to zero (see section 4b for complete details).

b. *Vorticity equation – Vorticity tendency*

Following R97, using the diagnosed vertical motion for each forcing in the complete vorticity equation,

$$\frac{\partial \zeta}{\partial t} = -\mathbf{V} \cdot \nabla (f + \zeta) + (f + \zeta) \frac{\partial \omega}{\partial p} - \omega \frac{\partial \zeta}{\partial p} - \left(\frac{\partial \omega}{\partial x} \frac{\partial v}{\partial p} - \frac{\partial \omega}{\partial y} \frac{\partial u}{\partial p} \right) + (\mathbf{k} \cdot \nabla \times \mathbf{F}) \quad (2)$$

contributions to vorticity tendency from each forcing can be obtained separately:

$$\left(\frac{\partial \zeta}{\partial t} \right)_{VA} = -\mathbf{V} \cdot \nabla (f + \zeta) + (f + \zeta) \frac{\partial \omega_{VA}}{\partial p} - \omega_{VA} \frac{\partial \zeta}{\partial p} - \left(\frac{\partial \omega_{VA}}{\partial x} \frac{\partial v}{\partial p} - \frac{\partial \omega_{VA}}{\partial y} \frac{\partial u}{\partial p} \right) \quad (3)$$

$$\left(\frac{\partial \zeta}{\partial t} \right)_{FR} = (\mathbf{k} \cdot \nabla \times \mathbf{F}) + (f + \zeta) \frac{\partial \omega_{FR}}{\partial p} - \omega_{FR} \frac{\partial \zeta}{\partial p} - \left(\frac{\partial \omega_{FR}}{\partial x} \frac{\partial v}{\partial p} - \frac{\partial \omega_{FR}}{\partial y} \frac{\partial u}{\partial p} \right) \quad (4)$$

$$\left(\frac{\partial \zeta}{\partial t} \right)_X = (f + \zeta) \frac{\partial \omega_X}{\partial p} - \omega_X \frac{\partial \zeta}{\partial p} - \left(\frac{\partial \omega_X}{\partial x} \frac{\partial v}{\partial p} - \frac{\partial \omega_X}{\partial y} \frac{\partial u}{\partial p} \right), X = LTA, LSH, LLH, OR \quad (5)$$

c. *Thermodynamic equation – Temperature tendency*

Using the diagnosed vertical motion for each forcing and the thermodynamic equation,

$$\frac{\partial T}{\partial t} = S\omega - \mathbf{V} \cdot \nabla T + \frac{\dot{q}}{c_p}, \quad (6)$$

contributions to the temperature tendency from each forcing can be obtained separately:

$$\left(\frac{\partial T}{\partial t}\right)_Y = S\omega_Y, \quad Y = VA, FR, OR \quad (7)$$

$$\left(\frac{\partial T}{\partial t}\right)_{TA} = S\omega_{LTA} - \mathbf{V} \cdot \nabla T \quad (8)$$

$$\left(\frac{\partial T}{\partial t}\right)_{LH} = S\omega_{LLH} + \left(\frac{\dot{q}}{c_p}\right)_{LH} \quad (9)$$

$$\left(\frac{\partial T}{\partial t}\right)_{SH} = S\omega_{LSH} + \left(\frac{\dot{q}}{c_p}\right)_{SH} \quad (10)$$

where TA denotes temperature advection, LH latent heating and SH sensible heating. It is to be noted that the contribution to temperature change for the three thermodynamic forcings (TA , LH and SH) are due in part to their three-dimensional distribution (through the vertical motion produced by their Laplacian as well as their local term).

d. Nonlinear balance equation - Height Tendency

A partition of the height tendencies is performed using a temporal differentiation of the nonlinear balance equation (e.g. Charney 1955) as in R97. First the diagnosed vorticity and its tendency for each forcing are used to calculate the streamfunction and its tendency by inverting the Laplacian operator in 11a and 11b, where C represents each forcing.

$$\nabla^2 \left(\frac{\partial \psi}{\partial t} \right)_C = \left(\frac{\partial \zeta}{\partial t} \right)_C, \quad C = VA, FR, OR, LTA, LSH, LSH \quad (11a)$$

$$\nabla^2 \psi = \zeta \quad (11b)$$

The height tendencies for each forcing are then obtained by inverting the Laplacian operator in (12), the non-linear balance equation (Charney, 1955).

$$g \nabla^2 \left(\frac{\partial Z}{\partial t} \right)_C = f \nabla^2 \left(\frac{\partial \psi}{\partial t} \right)_C + 2 \left[\frac{\partial^2}{\partial x^2} \left(\frac{\partial \psi}{\partial t} \right)_C \frac{\partial^2 \psi}{\partial y^2} + \frac{\partial^2 \psi}{\partial x^2} \frac{\partial^2}{\partial y^2} \left(\frac{\partial \psi}{\partial t} \right)_C - 2 \frac{\partial^2}{\partial x \partial y} \left(\frac{\partial \psi}{\partial t} \right)_C \frac{\partial^2 \psi}{\partial x \partial y} \right] + \beta \frac{\partial}{\partial y} \left(\frac{\partial \psi}{\partial t} \right)_C \quad (12)$$

where $\beta = df/dy$.

As reported by R97, this methodology for the height tendency provides good results except in the boundary layer because the nonlinear balance equation does not contain a frictional term. To avoid this problem in DIONYSOS the temporal differentiation of the hypsometric equation (13) is used to compute height tendencies in the boundary layer, which is arbitrarily defined as the 150 hPa layer above the surface p_{st} (see appendix Ad).

$$\left(\frac{\partial Z}{\partial t} \right)_{C_p} = \frac{R}{g} \int_p^{p_{st}-200} \left(\frac{\partial T}{\partial t} \right)_C \frac{dp}{p} + \left(\frac{\partial Z}{\partial t} \right)_{C_{p_{st}-200}} \quad (13)$$

This is accomplished by using the diagnosed temperature tendencies in the boundary layer and the diagnosed height tendencies at the first level above the boundary layer (p_{st} -200 hPa) in (13). In this way, the height tendencies in the boundary layer can be partitioned among the forcings without using (12) directly in the boundary layer.

e. Geostrophic Vorticity Tendency

Using the definition of the geostrophic vorticity, (14) is then used to calculate each forcing's contribution to the geostrophic vorticity tendencies.

$$\left(\frac{\partial \zeta_g}{\partial t}\right)_C = \frac{g}{f} \nabla^2 \left(\frac{\partial Z}{\partial t}\right)_C - \frac{g\beta}{f^2} \frac{\partial}{\partial y} \left(\frac{\partial Z}{\partial t}\right)_C \quad (14)$$

f. Divergence

Each forcing's contributions to the divergence can be obtained directly by using the continuity equation (15).

$$(\nabla \cdot \mathbf{V})_C = -\frac{\partial \omega_C}{\partial p} \quad (15)$$

g. *Lower and Upper Level Contribution*

In addition to the possibility of calculating the contribution of each forcing, the linear nature of the equations makes it also possible to compute the contribution of a forcing from a particular volume in the atmosphere to vertical motion, divergence, and tendencies of vorticity, height and temperature in any other part of the atmosphere. In the current version of DIONYSOS, contributions from the forcings are computed separately from low levels [1000 – 550 hPa] and from upper levels [500 – 100 hPa]. This is done simply by solving the equations using only the forcing from the computed layer while setting to zero the forcings in the other layer. Here again, when the omega equation (1) is solved, homogeneous conditions ($\omega=0$) are imposed on all (lateral, upper and lower) boundaries in both low level and upper level forcing cases except for the orographic contribution.

3. Ageostrophic vorticity tendency term

Traditionally the ageostrophic vorticity tendency in (1) has been either neglected (e.g., Gachon *et al.*, 2003; Lupo *et al.*, 1992)) or considered as an independent forcing term (e.g., R95; R97). Here an alternative approach is used, which consists of dividing the AG term among the forcings. This is accomplished by iterating. First the omega equation (1) is solved for each forcing by neglecting the AG term. Then equations (2-14) are used to calculate the vorticity tendencies (3, 4, 5), temperature tendencies (7, 8, 9), height tendencies (12, 13) and the geostrophic vorticity tendencies (14). Finally (16) is

used to calculate the ageostrophic vorticity tendency due to each forcing and reintroduced into (1).

$$\left(\frac{\partial \zeta_{AG}}{\partial t}\right)_C = \left(\frac{\partial \zeta}{\partial t}\right)_C - \left(\frac{\partial \zeta_G}{\partial t}\right)_C \quad (16)$$

This process is then repeated until the solution for omega converges.

Because friction near the ground systematically reduces the vorticity, an empirical approach is used to calculate the ageostrophic vorticity tendency in the boundary layer. Using the local ratio of the model vorticity tendency to the model geostrophic vorticity tendency, a frictional correction K is calculated¹ and assumed to be the same for each forcing. This ratio is then used in (17) to calculate the ageostrophic vorticity tendency for each forcing for grid points in the boundary layer.

$$\left(\frac{\partial \zeta_{AG}}{\partial t}\right)_C = (K - 1) \left(\frac{\partial \zeta_G}{\partial t}\right)_C \quad (17)$$

4. Parameterizations

Because standard numerical model output does not usually contain temperature tendencies due to diabatic effects nor tendencies due to turbulent fluxes, influences such as friction, orography and diabatic heating have been parameterized in a simplified manner that is as independent as possible of model parameterizations. In this way, DIONYSOS can be run with standard output from most NWP models.

a. Friction

The influence of friction in the boundary layer is computed from the model wind and model pressure gradients. The method assumes that the pressure gradient, Coriolis and friction forces are in equilibrium in the boundary layer, which leads to:

$$f \mathbf{k} \times \mathbf{V} + \nabla \Phi - \mathbf{F} = 0 \quad (19)$$

Since the wind speed and direction and the geopotential height are available from standard model output, the friction force (\mathbf{F}) can then be calculated for grid points in the boundary layer which, in DIONYSOS, is arbitrarily defined as the layer between the surface (p_{sl}) (see appendix Ad) and the pressure level 150 hPa above ($p_{sl} - 150$ hPa).

b. Orography

Effects of the topography are considered by first computing an orographical vertical motion at the surface from (20) (e.g., Haltiner and Williams, 1980, p.65-66), which assumes the air follows the terrain height (H).

$$\omega_s^{OR} = -g\rho_s (\mathbf{V}_s \cdot \nabla H) \quad (20)$$

¹ To prevent K of reaching unphysical values when the model geostrophic vorticity approach zero, any values of K below zero are set equal to zero and any values of K above one are set equal to one.

Subscript ‘s’ refers to variables defined at DIONYSOS surface level (see appendix Ad). The result is then ‘prescribed’ as the lower boundary condition at the ‘surface’ (p_{sl} , see appendix Ad) in (1), which is then solved with all forcing terms on the right set to zero to produce the orographic contribution to the vertical motion.

c. Diabatic heating

The effects of diabatic heating are divided in two distinct contributions: heating from condensation and sensible heating or cooling due to fluxes from the earth’s surface into the boundary layer. The effects of evaporative cooling and radiative warming or cooling are neglected.

The parameterization of latent heating uses the average precipitation rate computed from the model-accumulated precipitation. First the mean precipitation rate (PR) is converted in terms of a heating rate (\dot{Q}_{LH} , $\text{K kg m}^{-2} \text{s}^{-1}$) for the each grid point using:

$$\dot{Q}_{LH} = \rho_w \overline{PR} \cdot \frac{L_c}{c_p} \quad (21)$$

where L_c is the latent heat of condensation² and ρ_w (equal to 1000 kg m^{-3}) represents the conversion factor to transform the precipitation rate units from m s^{-1} to $\text{kg m}^{-2} \text{s}^{-1}$.

This heating rate is then distributed in the vertical according to the vertical profile of a ‘diabatic residual’ obtained by isolating the profile of the diabatic term in (6) in

² Currently, we are neglecting the small impact of freezing on the latent heat release in the cases of freezing precipitation.

which the model vertical motion ω is used. The horizontal temperature advection, static stability and the temperature tendency in (6) are also computed from model wind and temperatures. This ‘diabatic residual’, calculated at each grid point, is used to define the fraction of the overall heating rate that should be applied at each pressure level in the vertical. The latent heating at each pressure level is then calculated from

$$\left(\frac{\dot{q}_{LH}}{c_p} \right)_p = \frac{F_p}{D M} \dot{Q}_{LH} \quad (22)$$

where D is the total area under the curve defined by the ‘diabatic residual’ profile, F_p is the partial area of the ‘diabatic residual’ profile between the pressure level p and the level below ($p+50$ hPa), and M is the mass per unit of surface of a 50 hPa layer.

This method ensures that the vertical integral at each grid point of the latent heating is equal to the overall heating rate recovered from the mean precipitation. The ‘diabatic residual’, however, is put to zero at the surface level (p_{st} , see appendix Ad) and above the tropopause to avoid distributing latent heating at the surface and in the stratosphere. Also all negative residuals are set to zero ensuring that only heating is taken into account.

Parameterization of the sensible heating forcing follows a similar methodology to that for latent heating. The surface sensible heat flux from model output (h) is transformed into a heating rate (\dot{Q}_{SH} , $\text{K kg m}^{-2} \text{s}^{-1}$) according to:

$$\dot{Q}_{SH} = \frac{h}{c_p} \quad (23)$$

and this heating rate is then vertically distributed in the first 100 hPa following the vertical profile of the same ‘diabatic residual’ obtained with the thermodynamic equation (6)³. Elsewhere sensible heating is set to zero.

5. Diagnostic validation

The validity of the diagnostics can be assessed by comparing the total diagnosed vertical motion (sum of contributions from each forcing) as well as the diagnosed tendencies of vorticity, geopotential and temperature to the model values. Metrics used are spatial correlations between diagnosed fields and model output as well as a comparison of the root mean squares (rms) amplitudes. Validations are presented for both a winter case (from 1030 UTC 25 Dec to 1030 UTC 26 Dec 1999 initialized at 00 UTC 25 Dec) and a summer case (1030 UTC 15 Jun 2001 to 1030 UTC 16 Jun 2001 initialized at 00 UTC 15 Jun 2001) for diagnostics of the operational CMC GEM model (Côté *et al.* 1998a,b) output over Western Europe.

The GEM global model at that time was a 3D finite element, fully implicit and semi-Lagrangian model with 28 hybrid levels in the vertical run on a latitude/longitude/ grid with a horizontal resolution of 0.9°. The model data used for the diagnostics

³ In regions where both precipitation and warming due to sensible heat flux occurred, the same diabatical residual is used in the boundary layer to distribute each diabatic effects which can lead to an erroneous distribution of latent heating and sensible heating. We haven’t found yet a way to solve this problem. However it is believed to have a rather small negative impact on the quality of the results in general.

consisted of three hourly operational output interpolated on a 51 x 51 polar stereographic grid with 100 km horizontal resolution.

Figure 1 presents the synoptic situation for the two cases. The winter case represents the rapid development phase of windstorm ‘Lothar’ (Fig. 1a) over Western Europe. The summer case is the operational forecast of a weakening cyclone south of England and a developing Mediterranean system (Fig. 1b).

The average (over nine output times) correlation coefficients between the model and diagnosed parameters and a comparison of the rms for each variable for the two cases are presented in Figs. 2-7.

Similar statistics were also calculated for vertical motions calculated by neglecting the AG term in the omega equation (1) or by using an adiabatic and frictionless QG omega equation (24) (e.g. Bluestein, 1992 p.329),

$$\frac{R S}{p} \nabla^2 \omega + f^2 \frac{\partial^2 \omega}{\partial p^2} = -\frac{R}{p} \nabla^2 (-\mathbf{V}_G \cdot \nabla T) - f \frac{\partial}{\partial p} [-\mathbf{V}_G \cdot \nabla (f + \zeta_G)] \quad (24)$$

where the subscript G refers to geostrophic quantities.

a. Results

In general the correlation coefficients between model and diagnosed values for vertical motion (Figs. 2a and 3a), vorticity tendency (Fig. 4a), temperature tendency (Fig. 5a), height tendency (Fig. 6a) and geostrophic vorticity tendency (Fig. 7a) are between

0.85 and 0.95 throughout most of the atmosphere. In general the winter case shows slightly better correlations. The rms reveal, for their part, that the diagnostics fields reproduce very well the amplitudes of the model fields (Figs. 2b, 3b, 4b, 5b, 6b and 7b) at all levels with the exception of the temperature tendencies near the surface.

Statistical comparisons (Fig. 2a) for the diagnosed vertical motion with and without the AG term reveal that the inclusion of the AG term as a dependent forcing term (see section 3) increased the correlation mainly in the winter case, with a gain of 0.02 to 0.04 at most levels. The rms values show that the inclusion of the AG term moves the diagnosed values of vertical motion slightly closer to the model values, again mainly in the winter case. This is probably due to the fact that the winter case represents a case of a strong and fast moving system (thus generating important ageostrophic vorticity tendencies) while the summer case depicts the evolution of two weak and slow moving systems (thus generating little ageostrophic vorticity tendencies). It can be seen in Fig. 8d that, for the winter case, the AG term corrects mainly the diagnosed vertical motion locally in the region near the strong surface system (see Fig 1a) where ageostrophic vorticity tendencies are the strongest.

The QG diagnostics, however, are quite poor since the correlation never exceeds 0.85 and deteriorate significantly in the lower half of the troposphere (Fig. 2a and 3a). As for the rms, QG diagnosed vertical motions are systematically weaker than those of the model (Fig. 2b and 3b). The deterioration of the QG diagnostics in the low levels is due to two factors, both related to the effect of friction:

- a) The frictional forcing is not considered in (24).

b) Eq 24 used the geostrophic wind and the geostrophic vorticity instead of the total wind and total vorticity. This lead to an over-estimation of the wind speed and vorticity in the boundary layer leading to a deterioration of the diagnostics in the low levels. These facts have been investigated by Räisänen (1996).

b. Possible sources of the differences

Because of the approximations used to compute the diagnostics, they cannot be expected to reproduce perfectly the original model fields. The differences can be attributed to a number of sources whose individual contributions are difficult to isolate and quantify. Thus we can only speculated on these sources.

First, in order to run the diagnostics on standard model output, some of the forcings (friction, orography and diabatic effects) are parameterized using very simple formulations. A second source of possible error is the fact that the model fields are linearly interpolated between consecutives model output times, 3 hours apart, which essentially assumes that these fields are varying linearly over the period. Other tests have shown that this assumption cannot be used for 6 hourly model output. For higher spatial resolutions, periods shorter than 3 hours must be used. Another possible source of error is the nonlinear balance approximation. Finally there may be errors due to the use of homogenous boundary conditions that may occur whenever the average value of the parameter along the boundary is not zero.

6. Summary and discussion

A description of the diagnostic software DIONYSOS for the interpretation of weather systems from numerical simulations was presented. The diagnostic equations in DIONYSOS allow for the identification of individual dynamic and thermodynamic forcings, including their physical location, responsible for the development of (tendencies of vorticity, geostrophic vorticity, temperature and geopotential height), as well as vertical motion and divergence in model-simulated weather systems. The hydrostatic primitive omega, vorticity, and thermodynamic equations as well as the nonlinear balance equation form the core of the diagnostics. DIONYSOS was developed to be able to be run only using standard output from operational numerical models. This ability is made possible by the parameterization techniques implemented in DIONYSOS, which were developed in a simple manner in order to be independent of the individual model parameterization schemes. DIONYSOS computes the diagnostics at every 50 hPa in the vertical on interpolated data at intermediate times between consecutive model output. This procedure makes it possible to compare diagnosed and model tendencies. A new iterative methodology using the nonlinear balance approximation was also presented to include the AG term in the omega equation without calculating it as an independent forcing as in R97. Statistical comparisons between DIONYSOS diagnostics and model parameters for nine synoptic times from two 24-hour simulations (a winter case and a summer case) from the Canadian GEM model in its global configuration show very good agreement between the diagnostic and model fields. Our framework shows less departure

from the model values than QG, which reduces possible ambiguity in the interpretation of the physical processes.

Although the validation presented here is only for two cases, experience from the daily diagnostics from three different models from two different countries which are available on the web (<http://www.dionysos.uqam.ca>) has shown that these results are representative of the daily performance of the diagnostics. The comparison of vertical motion diagnostics calculated with and without the AG term showed that its inclusion only improves on the average the diagnostics slightly. However, its impact was concentrated around intense weather systems, which are often of considerable interests. Examples of the use of the current version of DIONYSOS can be found in Caron (2002), Caron *et al.* (2007a,b,c), Pagé *et al.* (2007) and, for an older version, in Gachon *et al.* (2003).

In the future, modifications will be made to test the diagnostics for higher resolution models. In addition, a potential vorticity inversion module using the assumption of nonlinear balance will be implemented in order to calculate the forcings from the potential vorticity.

Acknowledgements

The work presented in this paper was partially supported by the following organizations: Cooperative Program for Operational Meteorology, Education and Training (COMET), Natural Sciences and Engineering Research Council of Canada, Météo-France, Meteorological Service of Canada (MSC), and the Canadian Foundation for Climate and Atmospheric Sciences (CFCAS). The authors thank the large group of collaborators who have been involved throughout the years in the development or the validation of various aspects of previous versions of DIONYSOS: François Bonnardot, Pierre Bourgouin, Michel Desgagné, Serge Desjardins, Philippe Gachon, Olivier Hamelin, Pascale Roucheray, Judy St-James, Christian Viel and Pascal Yacouvakis.

APPENDIX A

Required data and processing

a. Data

The required set of data needed by DIONYSOS (Table A1) to compute all the diagnostics is relatively small and consists of model output generally made available by most modeling systems. It includes three-dimensional gridded values of u , v , T , Z , and ω on isobaric surfaces (or must be interpolated to isobaric surfaces) between 1000 hPa and 100 hPa at a maximum of 3 hour intervals. In addition, the sensible heat flux and accumulated precipitation is required at the model's surface as well as the model surface pressure and topography.

b. Preliminary processing – Interpolation

The model output is first linearly interpolated on 19 pressure levels at 50 hPa intervals, from 1000 hPa to 100 hPa on a polar stereographic grid with a horizontal resolution of 100 km. Next a linear temporal interpolation is used to calculate model data at intermediate times between two consecutive model output times. Diagnostic results are thus valid at these intermediate times (Fig. A1). This temporal interpolation is necessary because of the procedure used to parameterize diabatic effects (see section 4c). For example, the mean precipitation rate over a time interval is derived from the accumulated precipitation from two consecutive model output times. For comparison and

validation of the diagnostics, ‘model’ tendencies of vorticity, geostrophic vorticity, height and temperature are obtained using centered finite differences from consecutive model output.

c. Solving the equations

All derivatives are computed using centered finite differences, except for grid points at the borders of the grid where derivatives are computed using non-centered methods (forward or backward finite differences).

The omega equation used to diagnose vertical motion (1) is an elliptic partial differential equation. This equation is solved iteratively using three-dimensional sequential over-relaxation (Haltiner and Williams 1980) with homogenous boundary conditions ($\omega=0$) except for the calculation of the contribution of orography to the vertical motion. The iterative process is halted when the maximum differences in ω from two consecutive solutions is smaller than 10^{-4} Pa s⁻¹. The solution to equation will not converge when (1) is no longer elliptic which occurs when

$$S \leq 0 \tag{a1}$$

or

$$\frac{RSf}{p}(\zeta + f) \leq \frac{f^2}{4} \left| \frac{\partial \mathbf{V}}{\partial p} \right|^2 \tag{a2}$$

To ensure convergence in these situations, the stability (S) and/or relative vorticity (ζ) are slightly modified (following R95 rules, p.2450) when one or both conditions are met.

To invert the Laplacian for computing of height tendencies, streamfunction tendencies and the streamfunction, a two-dimensional version of the sequential over-relaxation method is used (Haltiner and Williams, 1980) with homogenous boundary conditions ($\partial Z/\partial t = 0$ and $\partial \psi/\partial t = 0$) for, respectively, the height and the streamfunction tendencies and $\psi = \phi/f$ as boundary conditions for the streamfunction.

d. Lower boundary

Because the isobaric model data below the model's topography is often unrealistic, the bottom boundary at each grid point is the isobaric level (to the nearest 50 hPa) just under the model's surface pressure (p_s).

e. Post processing – Filtering

The numerical computations of the numerous high-order partial derivatives generate a great deal of numerical noise that contaminates the results at the scale of several grid lengths. To remove the contaminated information, after all computations are performed, the results are spatially filtered by a Shuman filter (Shuman 1957, Shapiro 1964) that is configured so that wavelengths smaller than $6\Delta x$ (the grid length) are completely removed, while those larger than $14\Delta x$ are retained at more than 80% (Fig.

A2). For validation purposes the raw model output is also filtered the same way in order to maintain consistency when comparing the diagnostics to the model parameters.

In addition, the outer five horizontal grid points are removed to eliminate errors due to the homogenous horizontal boundary conditions and the propagation of these errors into the nearby interior due to the filtering.

REFERENCES

- Bluestein, H., 1992: *Synoptic-dynamic meteorology in midlatitudes*, Vol. I: *Principles of kinematics and dynamics*, Oxford University Press, 431 pp.
- Caron, J.-F., 2002: Étude diagnostique de la tempête de vent en Europe du 26 décembre 1999. Master's thesis, Department of Earth and Atmospheric Sciences, Université du Québec à Montréal.
- _____, M. K. Yau, S. Laroche, and P. Zwack, 2007a : The characteristics of key analysis errors. Part I: Dynamical balance and comparison with observations. *Mon. Wea. Rev.* (in press).
- _____, M. K. Yau, S. Laroche, and P. Zwack, 2007b : The characteristics of key analysis errors. Part II: The importance of the PV corrections and the impact of balance. *Mon. Wea. Rev.* (in press).
- _____, M. K. Yau and S. Laroche, 2007c : The characteristics of key analysis errors. Part III: A diagnosis of their evolution. *Mon. Wea. Rev.* (in press).
- Charney, J., 1955: The use of the primitive equations of motion in numerical prediction, *Tellus*, **7**, 22-26.

Côté, J., S. Gravel, A. Méthot, A. Patoine, M. Roch and A. Staniforth, 1998a: The operational CMC-MRB global environmental multiscale (GEM) model: Part I - Design considerations and formulation, *Mon. Wea. Rev.*, **126**, 1373-1395

_____, J.-G. Desmarais, S. Gravel, A. Méthot, A. Patoine, M. Roch and A. Staniforth, 1998b: The operational CMC-MRB global environmental multiscale (GEM) model: Part II - Results, *Mon. Wea. Rev.*, **126**, 1397-1418

Gachon, P., R. Laprise, P. Zwack and F.J. Saucier, 2003: The effects of interactions between surface forcings in the development of a model-simulated polar low in Hudson Bay, *Tellus*, **55A**, 61-87

Haltiner, G.J., and R.T. Williams, 1980: *Numerical prediction and dynamical meteorology*, 2d ed. John Wiley & Sons, New York, 477 pp.

Holton, J.R., 1992: *An introduction to dynamic meteorology*. 3d ed. Academic Press, 511 pp.

Krishnamurti, T.N., 1968: A diagnostic model for studies of weather systems of low and high latitudes, Rossby number less than 1, *Mon. Wea. Rev.*, **96**, 197-207

Lupo, A.R., P.J. Smith and P. Zwack, 1992: A diagnosis of the explosive development of two extratropical cyclones, *Mon. Wea. Rev.*, **120**, 1490-1523

- Pagé, C., L. Fillion and P. Zwack, 2007: Diagnosing summertime mesoscale vertical motion: Implications for atmospheric data assimilation. *Mon. Wea. Rev.* (in press).
- Petterssen, S., 1956: *Weather analysis and forecasting*. Vol. I. 2d ed. McGraw-Hill, 428 pp.
- Räisänen, J., 1995: Factors affecting synoptic-scale vertical motions: A statistical study using a generalized omega equation. *Mon. Wea. Rev.*, **123**, 2447-2460
- Räisänen, J., 1996: Effect of Ageostrophic Vorticity and Temperature Advection on Lower-Tropospheric Vertical Motions in a Strong Extratropical Cyclone. *Mon. Wea. Rev.*, **124**, 2607-2413
- , 1997: Height tendency diagnostics using a generalized omega equation, the vorticity equation, and a nonlinear balance equation. *Mon. Wea. Rev.*, **125**, 1577-1597
- Shuman, F.G., 1957: Numerical methods in weather prediction: II Smoothing and filtering, *Mon. Wea. Rev.*, **85**, 357-361

Shapiro, R., 1970: Smoothing, filtering and boundary effects. *Rev. Geophys. and Space Phys.*, **8**, 359-387

Zwack, P., and B. Okossi, 1986: A new method for solving the quasi-geostrophic omega equation by incorporating surface pressure tendency data. *Mon. Wea. Rev.*, **114**, 655-666

Figure Captions

Figure 1. Synoptic situation over Western Europe from the Canadian GEM global forecast model simulation, after interpolation and filtering. Mean sea level pressure (solid lines, contour interval 4 hPa) and 500 hPa geopotential height fields (dashed lines, contour interval 6 dam) for a) 2230 UTC 25 Dec 1999, model initialized at 00 UTC 25 Dec 1999 and b) 2230 UTC 15 Jun 2001, model initialized at 00 UTC 15 Jun 2001.

Figure 2. Statistics for vertical motion averaged over 9 synoptic times of three hour intervals for a winter case (from 1030 UTC 25 Dec to 1030 UTC 26 Dec 1999). (a) Correlation coefficient between the model and the total diagnosed vertical motion (ω) for diagnostics including the AG term as presented in section 3 (\circ), diagnostics without the AG term (\diamond) and QG diagnostics (\square). (b) Root mean square ($10^{-1} \text{ Pa s}^{-1}$) for the model (\triangle) and the total diagnosed vertical motions with the AG term (\circ), without the AG term (\diamond) and QG (\square).

Figure 3. The same as Fig. 2, but for a summer case (1030 UTC 15 Jun 2001 to 1030 UTC 16 Jun 2001).

Figure 4. Statistics for vorticity tendency (diagnostics including the AG term in the omega equation as presented in section 3) averaged over 9 synoptic times of three hour intervals for a winter case (from 1030 UTC 25 Dec to 1030 UTC 26 Dec 1999) and a summer case (1030 UTC 15 Jun 2001 to 1030 UTC 16 Jun 2001). (a) Correlation coefficient between the model and the total diagnosed vorticity tendency for winter case (\circ) and summer case (\square) and (b) root mean square (10^{-9} s^{-2}) for the model (winter case (\diamond) and summer case (\triangle)) and the total diagnosed (winter case (\circ) and summer case (\square)) vorticity tendencies.

Figure 5. The same as Fig. 4, but for temperature tendency. (a) Correlation coefficient between the model and the total diagnosed temperature tendency and (b) root mean square (10^{-5} K s^{-1}) for the model (winter case (\diamond) and summer case (\triangle)) and the total diagnosed (winter case (\circ) and summer case (\square)) temperature tendencies.

Figure 6. The same as Fig. 4, but for height tendency. (a) Correlation coefficient between the model and the total diagnosed height tendencies and (b) root mean square ($10^{-5} \text{ dam s}^{-1}$) for the model (winter case (\diamond) and summer case (\triangle)) and the total diagnosed (winter case (\circ) and summer case (\square)) height tendencies.

Figure 7. The same as Fig. 4, but for geostrophic vorticity tendency. (a) Correlation coefficient between the model and the total diagnosed height tendencies and (b) root mean square (10^{-9} s^{-2}) for the model (winter case (\diamond) and summer case (\triangle)) and the total diagnosed (winter case (\circ) and summer case (\square)) height tendencies.

Figure 8. Vertical motion (ω -contour $0,1 \text{ Pa s}^{-1}$) at 700 hPa for the winter case at 2230 UTC 26 Dec 1999. a) Model output, b) total diagnosed forcing contribution with the AG term as presented in section 3, c) total diagnosed forcing contribution without the AG term and d) difference between panel b) and c).

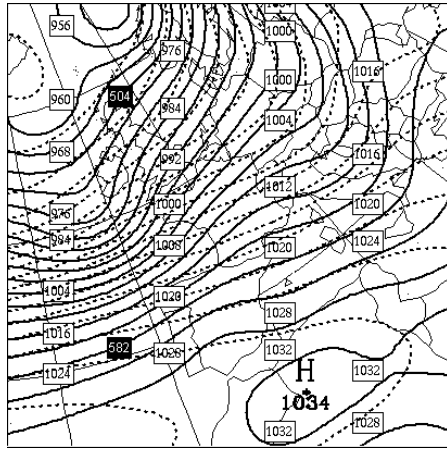
Figure A1. Forecast model data input time and time of validity of DIONYSOS diagnostics. Δt is the time interval between the model output.

Figure A2. Theoretical response of the two-dimensional Shuman filter after 42 iterations for $\lambda_x = \lambda_y$.

Table Captions

Table A1. Input data required by DIONYSOS

a) Winter Case



b) Summer Case

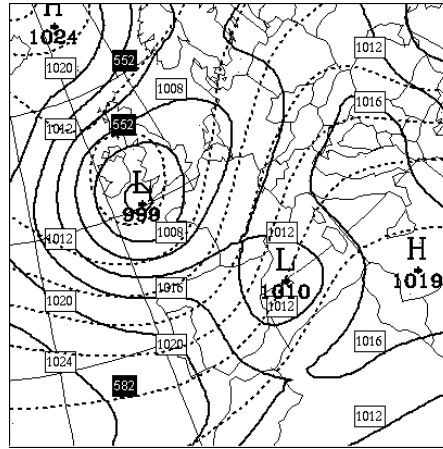


Figure 1. Synoptic situation over Western Europe from the Canadian GEM global forecast model simulation, after interpolation and filtering. Mean sea level pressure (solid lines, contour interval 4 hPa) and 500 hPa geopotential height fields (dashed lines, contour interval 6 dam) for a) 2230 UTC 25 Dec 1999, model initialized at 00 UTC 25 Dec 1999 and b) 2230 UTC 15 Jun 2001, model initialized at 00 UTC 15 Jun 2001.

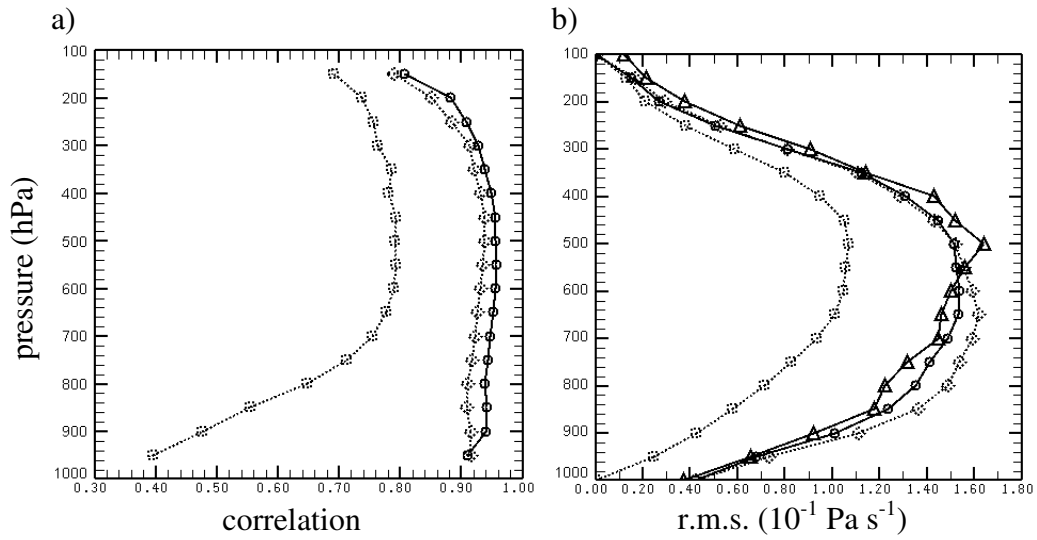


Figure 2. Statistics for vertical motion averaged over 9 synoptic times of three hour intervals for a winter case (from 1030 UTC 25 Dec to 1030 UTC 26 Dec 1999). (a) Correlation coefficient between the model and the total diagnosed vertical motion (ω) for diagnostics including the AG term as presented in section 3 (○), diagnostics without the AG term (◇) and QG diagnostics (□). (b) Root mean square ($10^{-1} \text{ Pa s}^{-1}$) for the model (△) and the total diagnosed vertical motions with the AG term (○), without the AG term (◇) and QG (□).

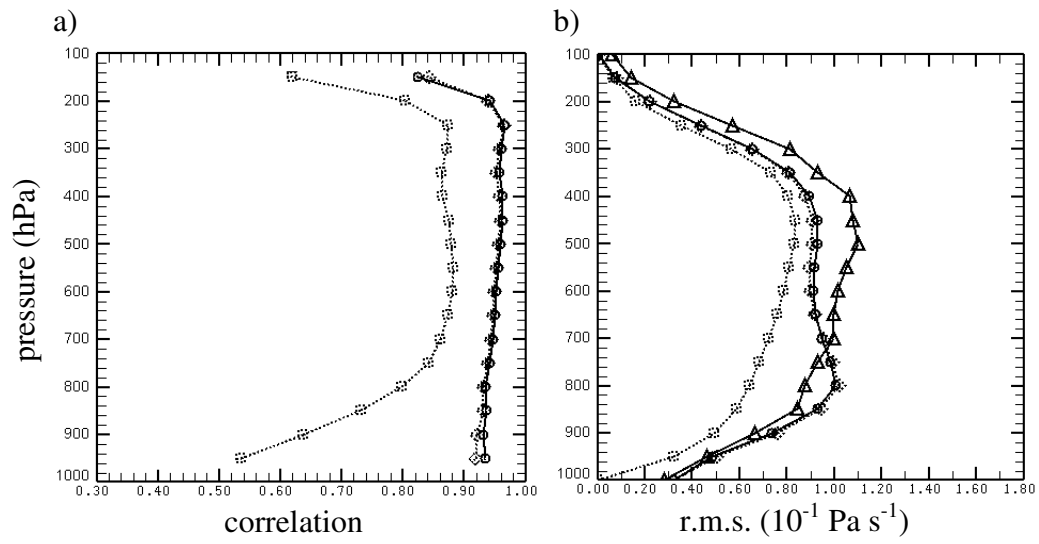


Figure 3. The same as Fig. 2, but for a summer case (1030 UTC 15 Jun 2001 to 1030 UTC 16 Jun 2001).

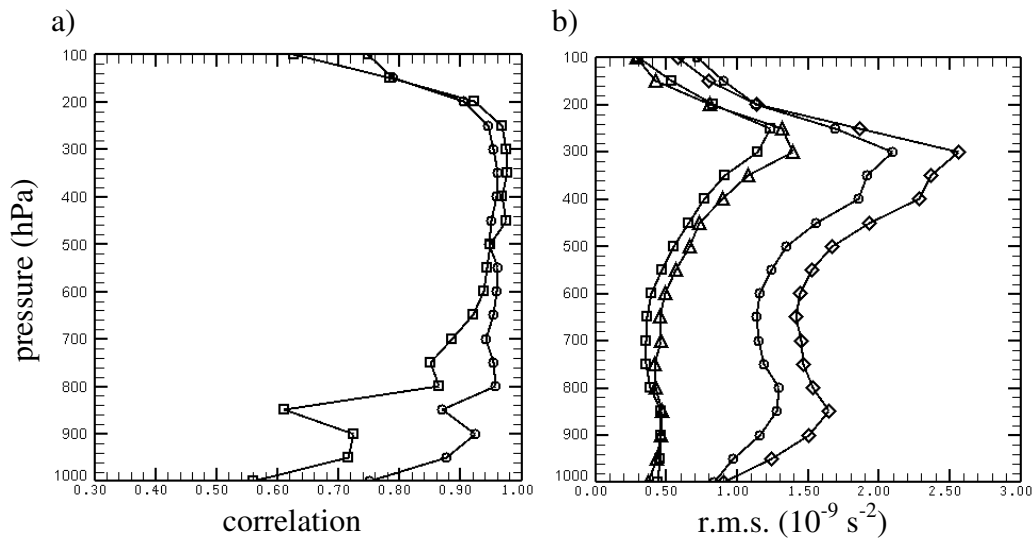


Figure 4. Statistics for vorticity tendency (diagnostics including the AG term in the omega equation as presented in section 3) averaged over 9 synoptic times of three hour intervals for a winter case (from 1030 UTC 25 Dec to 1030 UTC 26 Dec 1999) and a summer case (1030 UTC 15 Jun 2001 to 1030 UTC 16 Jun 2001). (a) Correlation coefficient between the model and the total diagnosed vorticity tendency for winter case (○) and summer case (□) and (b) root mean square (10^{-9} s^{-2}) for the model (winter case (◇) and summer case (△)) and the total diagnosed (winter case (○) and summer case (□)) vorticity tendencies.

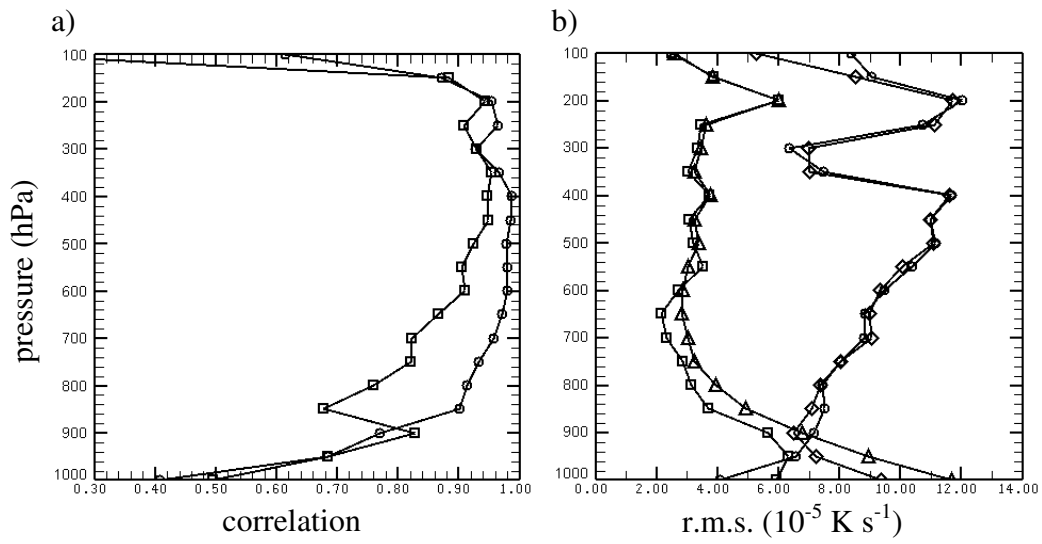


Figure 5. The same as Fig. 4, but for temperature tendency. (a) Correlation coefficient between the model and the total diagnosed temperature tendency and (b) root mean square (10^{-5} K s^{-1}) for the model (winter case (\diamond) and summer case (\triangle)) and the total diagnosed (winter case (\circ) and summer case (\square)) temperature tendencies.

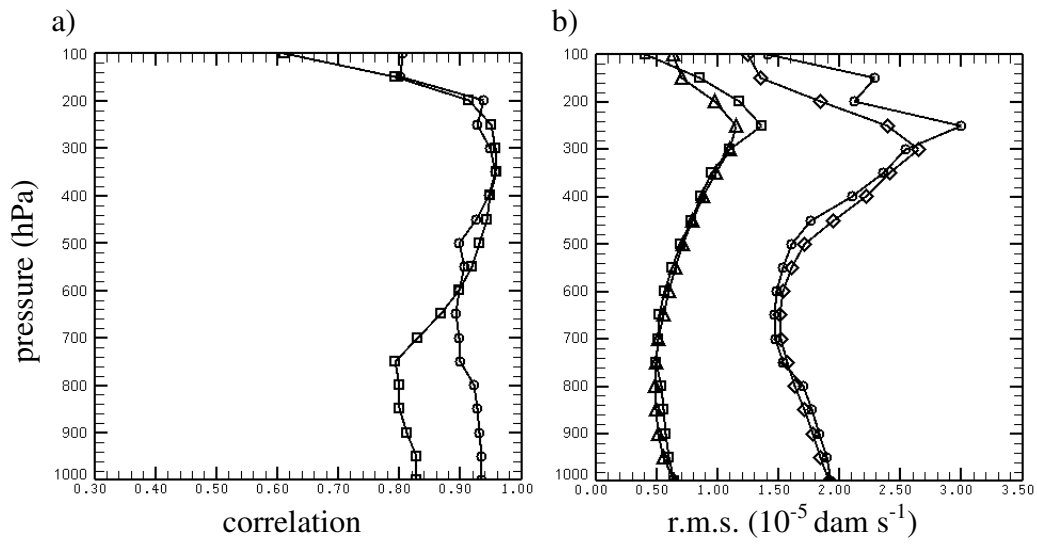


Figure 6. The same as Fig. 4, but for height tendency. (a) Correlation coefficient between the model and the total diagnosed height tendencies and (b) root mean square ($10^{-5} \text{ dam s}^{-1}$) for the model (winter case (◇) and summer case (△)) and the total diagnosed (winter case (○) and summer case (□)) height tendencies.

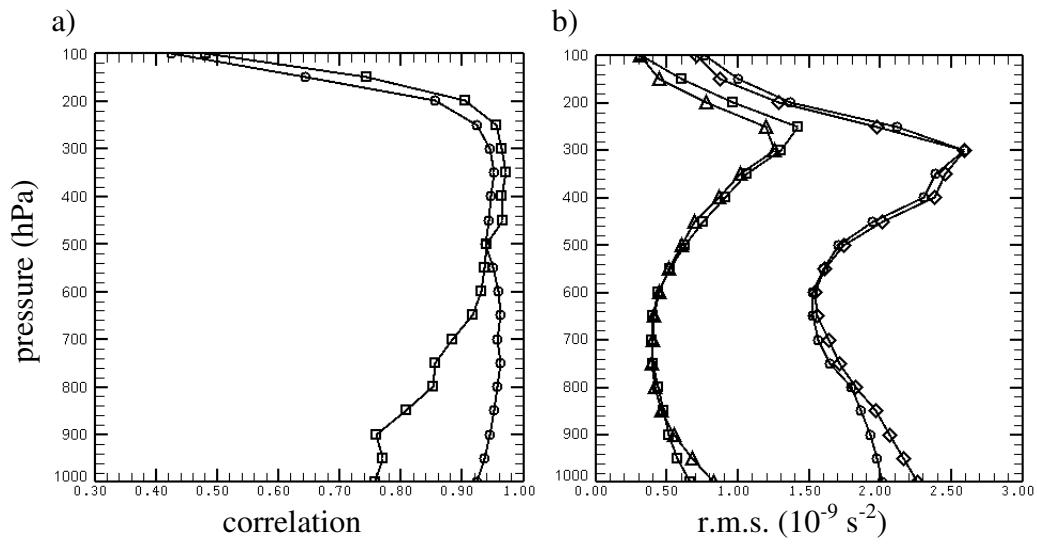


Figure 7. The same as Fig. 4, but for geostrophic vorticity tendency. (a) Correlation coefficient between the model and the total diagnosed height tendencies and (b) root mean square (10^{-9} s^{-2}) for the model (winter case (\diamond) and summer case (\triangle)) and the total diagnosed (winter case (\circ) and summer case (\square)) height tendencies.

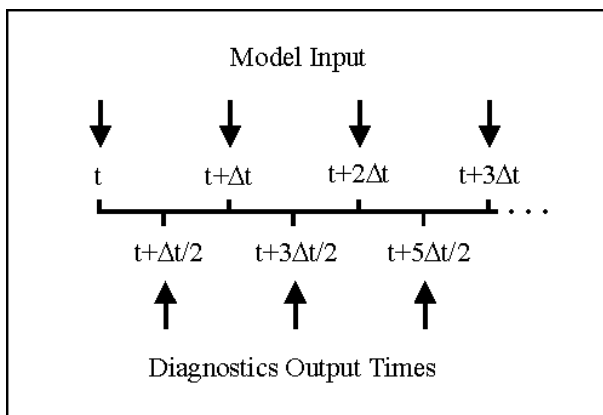


Figure A1. Forecast model data input time and time of validity of DIONYSOS diagnostics. Δt is the time interval between the model output.

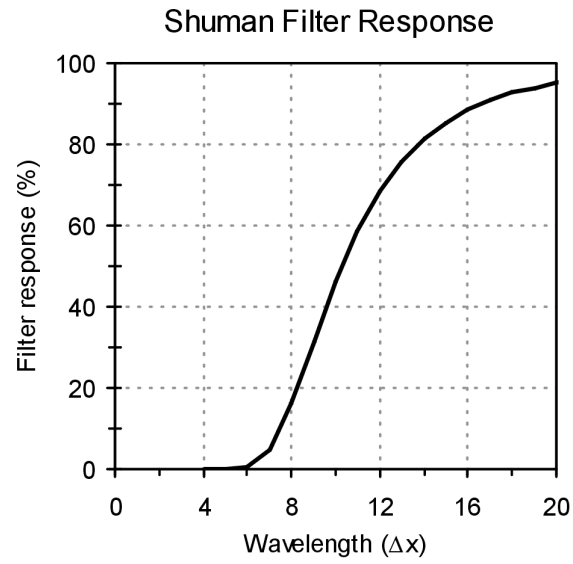


Figure A2. Theoretical response of the two-dimensional Shuman filter after 42 iterations for $\lambda_x = \lambda_y$.

TABLE A1. Input data required by DIONYSOS

Variables	Units
Wind 'x' (u)	knots
Wind 'y' (v)	knots
Temperature (T)	°C
Geopotential height (Z)	dam
Vertical motion (ω)	Pa s ⁻¹
Surface sensible heat flux (h)	J m ⁻² s ⁻¹
Precipitation accumulation	m
Surface pressure (p_s)	hPa
Geopotential topography (H)	m